Optimized 3D Gaussian Splatting using Coarse-to-Fine Image Frequency Modulation

Umar Farooq, Jean-Yves Guillemaut, Adrian Hilton, Marco Volino CVSSP, University of Surrey

{m.farooq, j.guillemaut, a.hilton, m.volino}@surrey.ac.uk



Figure 1. Opti3DGS progressively grows levels to reduce redundant and unused Gaussians while maintaining accurate geometric structure and competitive quality.

Abstract

The field of Novel View Synthesis has been revolutionized by 3D Gaussian Splatting (3DGS), which enables high-quality scene reconstruction that can be rendered in real-time. 3DGS-based techniques typically suffer from high GPU memory and disk storage requirements which limits their practical application on consumer-grade devices. We propose Opti3DGS, a novel frequency-modulated coarse-tofine optimization framework that aims to minimize the number of Gaussian primitives used to represent a scene, thus reducing memory and storage demands. Opti3DGS leverages image frequency modulation, initially enforcing a coarse scene representation and progressively refining it by modulating frequency details in the training images. On the baseline 3DGS [9], we demonstrate an average reduction of 62% in Gaussians, a 40% reduction in the training GPU memory requirements and a 20% reduction in optimization time without sacrificing the visual quality. Furthermore, we show that our method integrates seamlessly with many 3DGS-based techniques [4, 5, 12, 15, 19], consistently reducing the number of Gaussian primitives while maintaining, and often improving, visual quality. Additionally, Opti3DGS inherently produces a level-of-detail scene representation at no extra cost, a natural byproduct of the optimization pipeline. Results and code will be made publicly available.

1. Introduction

Photorealistic scene reconstruction remains a fundamental challenge in 3D computer vision, with applications spanning augmented and virtual reality, media production, and immersive gaming. Despite significant advancements, existing Novel View Synthesis (NVS) methods - particularly those based on Neural Radiance Fields (NeRF) [16] - face substantial computational constraints [2, 8, 13]. These constraints hinder broader adoption, especially on web, mobile, and edge devices, where efficient rendering and low memory usage are critical.

3D Gaussian Splatting (3DGS) [9], recently introduced as an explicit point-based NVS technique, achieves high

visual fidelity with fast training and real-time rendering. However, it suffers from significant GPU memory and storage overhead [18, 19], limiting its applicability across diverse device form factors.

To address these challenges we introduce Opti3DGS, a novel and efficient coarse-to-fine optimization strategy that reduces the number of Gaussians used to represent a scene. This translates into reduced memory and storage overheads compared to 3DGS [9]. Our approach begins with intentional over-reconstruction, which serves as an effective regularizer, followed by progressive refinement of the scene to balance detail and efficiency. Several techniques have been proposed which aim to reduce 3DGS memory and storage costs. Some focus on compressing the stored representation [3, 12, 14, 17, 18], others optimize training speed and parallelization [22], while a few attempt to minimize Gaussian primitive count during optimization itself [12, 19]. Our approach falls into the latter category, reducing Gaussian primitives during the optimization process, thereby decreasing GPU memory demands and accelerating training without sacrificing visual quality. Notably, our method achieves these benefits without introducing additional learnable parameters or requiring lengthy optimizations.

Opti3DGS improves the baseline 3DGS [9], achieving a 62% reduction in Gaussian primitives, a 40% decrease in GPU memory usage during training, and a 20% speedup in optimization time. Our technique is highly modular and can be easily incorporated into most 3DGS-based pipelines with minimal modifications. Furthermore, we demonstrate its positive impact when integrated into advanced 3DGS methods such as MiniSplatting [4] and Taming3DGS [15], as well as other recent appraches [5, 12, 19]. Due to the coarse-to-fine nature of our approach, it naturally produces level-of-detail representation as a byproduct, shown in Figure 1. To summarize, our key contributions are:

- We present Opti3DGS, a framework to minimize the number of Gaussian primitives in a 3DGS scene resulting in improved training speed, memory and storage requirements.
- We propose a coarse-to-fine optimization strategy that increases the size of the Gaussians at the start of optimization and then slowly breaks down the large coarse Gaussians in a controlled fashion leading to an improved Gaussian densification process.
- We demonstrate that Opti3DGS can be seamlessly integrated into a wide range of existing 3DGS techniques minimizing the number of Gaussians used to represent the scene without sacrificing visual quality, and in most cases improving it.

2. Related Work

3DGS Compression: One branch of approaches that aim to reduce the storage size of 3DGS scenes focuses on quan-

tizing raw parameters stored for each Gaussian primitive [3, 12, 14, 17, 18]. These enable efficient storage and transmission but since the optimization is done after 3DGS scene optimization, it does not lower GPU memory requirements during training and some require cumbersome decoding in GPU memory from a compressed representation which can be computationally expensive to render [10]. Some methods like [5] also include an efficient encoding and decoding mechanism for parameters during the optimization process, leading to both storage and compute time gains. However, in the case of [5] they use a separate neural network to decode the color values and face complications due to quantized vectors not being differentiable. A subset of these methods [4, 18-20] also compute the rendering importance of each Gaussian primitive based on its contribution to individual pixels, its relative size or the Gaussian neighborhood it is located in.

Gaussian Primitive Reduction: An alternative approach is to actively reduce the number of primitives during the optimization process [4, 12, 15, 19]. The Adaptive Density Control (ADC) mechanism in [9] removes Gaussians below a fixed opacity threshold at predefined intervals and densifies ones with large gradients by either splitting or cloning them. But despite these measures the primitive count increases rapidly and with much variation across runs. [12] proposed to learn a volume aware mask during training, incurring additional learnable parameters and optimization time, to remove primitives which are either small or have minimal contribution. But this approach is limited in its effectiveness because the problem stems from dense clustering of Gaussians in certain locations with a significant number of them not even contributing to the color at all [4, 18]. [4] show that there are multi-view inconsistencies between the centroids of the Gaussians and their location density is not uniform even in areas with uniform color and texture attributes and propose to regularize this inconsistency. [19] prunes Gaussians during the optimization process based on their rendering importance and signs of local clustering, however they do not reduce the peak GPU memory requirements during the optimization process. [15] propose the use of per-view per-pixel saliency maps to guide the densification process in a selective manner with predictable growth trend and used fused operations to speed up optimization. However all of these approaches require major changes in the ADC functionality and thus are not easily inter-compatible with each other and have unknown effects if combined.

Summary: We propose Opti3DGS, a coarse-to-fine frequency modulation approach to reduce the number of Gaussians by only changing the training images during the optimization process. [5] also use a coarse-to-fine strategy but the downsize images in resolution progressively, in contrast Opti3DGS modulates the image frequency. Both ap-

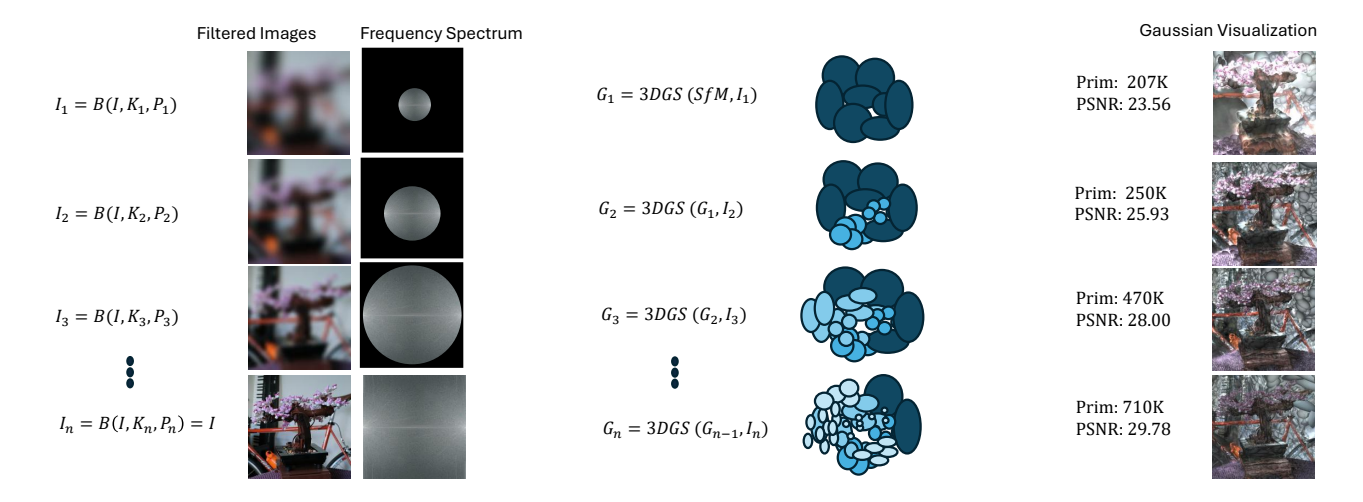


Figure 2. Method Overview: We start the optimization with very large and coarse Gaussians which are then densified based on the differentiable rendering signal. Specifically we control the frequency spectrum of the training images, gradually increasing the threshold for the low pass filtering.

proaches have a distinct impact on the image pixels and quite different results. [21] also use a frequency-based approach for optimizing 3DGS but they provide gradient signals in multiple separate frequency bands simultaneously with the goal of increasing visual quality which leads to a significantly higher Gaussian count. Opti3DGS on the other hand sits behind the ADC and is not directly involved in the differential rendering process. This ensures wide ranging compatibility with most 3DGS based methods and allows Opti3DGS to integrate with compression and quantization-based methods. Opti3DGS also directly minimize the Gaussians which leads to reduced GPU memory requirements while the optimization process is still ongoing.

3. Method

3.1. Preliminaries: 3D Gaussian Splatting

3DGS [9] uses anisotropic Gaussians whose shape, color, opacity and refraction parameters are estimated via multiview image-based optimization. Each Gaussian is defined by a covariance matrix Σ , a center position \mathbf{p} , opacity α , and spherical harmonics coefficients for color \mathbf{c} . The covariance matrix Σ is decomposed into a scaling matrix and a rotation matrix to facilitate differentiable optimization. For rendering, all Gaussians in the view frustum are splatted using onto a 2D plane followed by α -blending of the color based on Gaussian opacity to achieve the final image. The color C of a pixel is computed by blending N ordered 2D Gaussians that overlap the pixel, formulated as:

$$C = \sum_{i \in N} c_i \alpha_i \prod_{j=1}^{i-1} (1 - \alpha_j)$$
 (1)

Here, the final color c_i of a pixel is defined by the color of each Gaussians, dependent on the spherical harmon-

ics based on the view direction, falling on to the specific pixel multiplied by its individual opacity and the cumulative opacity α_i of the i Gaussians in front. This approach ensures that the contributions of overlapping Gaussians are blended accurately, resulting in a precise and realistic rendered image of the scene. The implementation also allows gradients to pass to an unrestricted number of Gaussians at any depth behind the camera position. Over the course of optimization, numerous tiny changes based on the gradients from differential rendering of multi-view images allow for the Gaussians to approximate shapes and colors close to real scene geometry.

3.2. Opti3DGS Overview

Our approach, shown in Figure 2, controls the frequency information in the training images which has a downstream effect on the ADC mechanism by providing it with a streamlined loss landscape. Starting with low frequency details in the scene, it steers the densification process to first approximate the large scale structure of the scene using large and coarse Gaussians, as shown in Figure 1. This also alleviates the pressure on the ADC to densify the image in regions with highly dense initial Structure-from-Motion (SfM) points, as shown in Figure 3. This indirect modulation signal allows the optimizer to approach a desirable balance between focusing on under and over-reconstructed regions of the scene.

3.3. Image Frequency Modulation

Digital images are made up of a spectrum of frequencies representing the structure and pattern of the color in them, with low frequencies corresponding to structure in the pixel space with gradual changes and high frequencies represent-

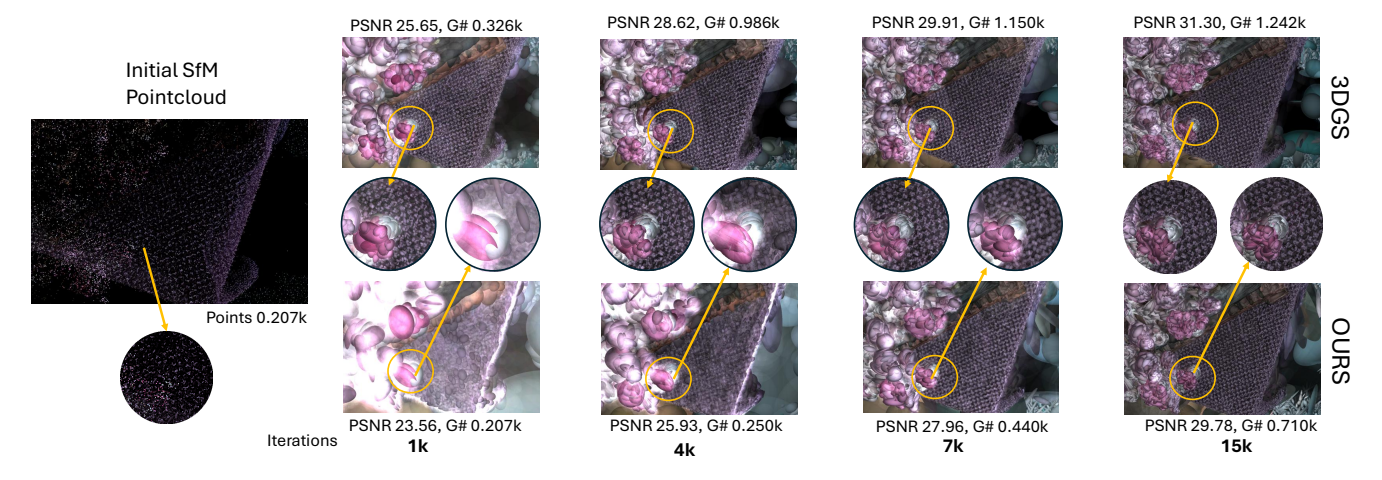


Figure 3. We start with uniform distribution of larger Gaussians as compared to 3DGS which starts heavy densification from the very start of optimization thus complicating the loss landscape. The zoomed views show efficient use of the initial sparse pointcloud by our approach.

ing frequently changing color patterns like textures or white noise. There are a number of techniques for manipulating, enhancing or removing signals in different parts of the frequency spectrum depending on the downstream use-cases. Conceptually, a simple way of removing high frequency signals from an image exploits the local relation between pixels in a neighborhood to tease out only the consistent and stable color structures. The opposite can be thought to remove low frequency signals, but in practice a wide range of mathematical and statistical machinery is employed to perform various frequency restriction operations on images in an efficient fashion. Opti3DGS uses frequency manipulation on the training images as a tool to control the size of the Gaussians and deals with low pass filters, which only keep low frequencies or large scale structures while discarding high frequencies containing texture patterns and noise components. We experiment with mean, bi-lateral, Gaussian and Sobel filtering techniques in our approach and demonstrate that mean filtering is the most effective, shown in Section 4.3. A simple low pass filtering operation on an image can be described as:

$$G[i,j] = \sum_{u=-k}^{k} \sum_{v=-k}^{k} H[u,v]F[i-u,j-v]$$
 (2)

where H and F represent the convolutional kernel and the input image respectively with G being the resulting image from the operation. Importantly, we fix the stride to 1 for all our experiments and adjust the padding to ensure the spatial dimensions of the image don't change during any step of the image processing pipeline. The values in the filtering kernel in the context of a convolution operation define the type of filtering that will happen to the image. Gaussian kernels emphasize the central values in the filtering window of the image whereas a mean filter weighs them equally.

3.4. Frequency Training Schedule

Starting with very large coarse Gaussians and progressively adding high frequency details requires a schedule of frequency removal and addition. We define various mechanisms, including linear, cosine, cosine restarting, exponential and step functions, as shown in Figure 4, which control the intensity of the image frequency modulation given the current training iteration as input. For the step function we define a single value for a fixed iteration interval and define all intervals accordingly. Based on ablation experiments, described in Section 4.3, the step function to be most effective.

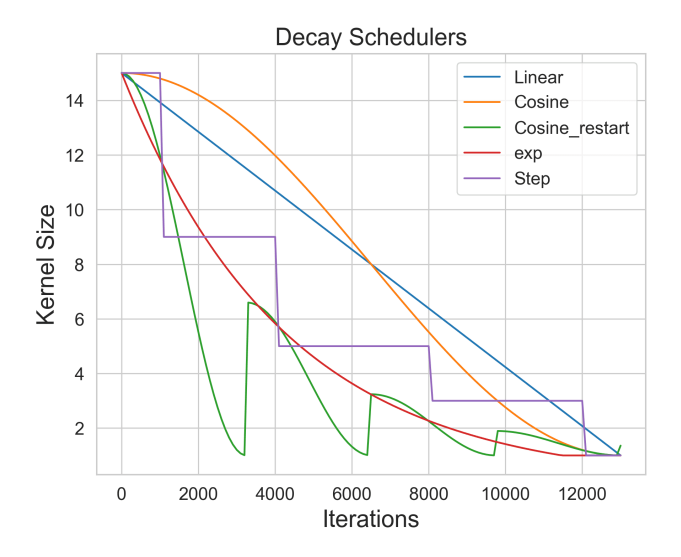


Figure 4. Visualization of different decay rates reported in our work. The vertical axis shows the current kernel size for the filtering algorithm for any given iteration. Note we stop all frequency modulation after 12,000 iterations and pass full sized images for the remaining 18,000 iterations.

3.5. Progressive Growing Pipeline

Opti3DGS employs a progressive frequency control strategy with five distinct image and scene quality levels I_n and G_n respectively in range n=(1-5) as depicted in Fig.1. We start by first obtaining a sparse scene reconstruction and initial 3D points using SfM on the training images I and this initial sparse representation acts as our G_0 at n=0 for initializing the Gaussians.

$$G_0 = SfM(I) \tag{3}$$

Then for each subsequent level in our coarse-to-fine optimization process we use the last set of Gaussians G_{n-1} as the starting point and the normal 3DGS optimization loss is used to optimize G_{n-1} using the filtered images I in range n=(1-5).

$$G_n = 3DGS(G_{n-1}, I_n) \tag{4}$$

where the images I_n are obtained from the filtering function $B(I, K_n, P_n)$. For each level the images get progressively sharper and more high frequency content is allowed to remain in the image. For the last level, n=5, we directly pass the original training images to the 3DGS optimizer.

$$G_5 = 3DGS(G_4, I) \tag{5}$$

For level-of-detail representation results, the model is saved at the last iteration before transitioning to the next level.

4. Results and Evaluation

Datasets: Following common practice we use the Mip-NeRF360 [1], DeepBlending [7] and Tanks and Temples [11] datasets with a total of 13 scenes including a good mix of indoor and outdoor unbounded scenes. We use the train and truck scene from [11], the drjohnson and playroom scene from [7] and bicycle, bonsai, treehill, counter, kitchen, stump, flowers, garden and room scenes from [1]. **Implementation Details**: All our ablations, graphs and results are reported as the average scores for all held-out test views averaged for all 13 scenes, with the exception of Figure 1 and Figure 5 which report the results averaged for all test views for the bicycle scene. For testing the impact of our module on top of other 3DGS based methods, we first reproduce the software environment and reported results from the authors and then re-run the code with our changes applied using the authors provided training and evaluation scripts for fair comparison and evaluation. We do not change any hyper-parameters or settings for any of the methods except for 3DGS [9] where we change the scaling_lr= 0.01, densification_interval= 500 and densify_grad_treshold= 0.0001. All experiments and comparison were undertaken using a NVidia H200 GPU. We use the step decay function as shown in Figure 4 with a mean blur filter with an initial kernel size of 15 in all our experiments and stop frequency modulation after the first 12,000 iterations. Further ablations of these parameters are presented in Section 4.3. Reconstructed scene models and code to reproduce results will be made publicly available.

Metrics: We use PSNR, SSIM and LPIPS for quantitative evaluation and analysis of the trained models and for reproducing relevant baselines. We follow the established best practice of keeping every 8^{th} frame for a hold-out test set and train all our experiments for 30,000 iterations and comply with the image resolution convention from [9] for using full scale images for DeepBlending [7] and Tanks and Temples [11] and using 2^{nd} and 4^{th} image resolution levels after Colmap processing for MipNeRF360 [1] indoor and outdoor scenes respectively.

4.1. Progressive Growing Impact

Our approach achieves excellent reduction in the number of Gaussians used to represent a scene while maintaining competitive visual quality or improving the visual quality. We achieve a reduction in the number of Gaussians in all datasets for each of the methods as reported in Table 1, which is impressive given that all listed methods aim to reduce the file size and Gaussian count and are already extremely efficient. For some methods, such as MiniSplatting [4] and Compact3DGS [12], the final Gaussian count is not a true representation of the GPU memory requirements as that peaks at various points during training. Opti3DGS also reduces the peak Gaussian load as well as the final Gaussian count for both MiniSplatting[4] and Compact3DGS[12] as reported in Table 1. A reduction in the number of Gaussians during the optimization process also leads to accumulated speedups in terms of optimization time as reported in Table 1 and shown in the Figure 6.

We also compare Opti3DGS against the approach used by EAGLES [5] in their coarse-to-fine training strategy where they reduce the image resolution to get a coarse scene representation. However, our approach maintains the full image resolution during the entire image processing pipeline and we show the visual comparison for this in our supplementary material. When isolated, the coarse-to-fine approach from [5], is outperformed by Opti3DGS as reported in Table 2, where we apply both techniques to 3DGS [9] to tease out their impact. Note that we have better reconstruction across the board for all datasets while maintaining equally competitive Gaussian counts. Additionally, if we substitute our frequency modulation approach in the full pipeline from EAGLE [5] as reported in Table 1 there is a positive improvement in results while the Gaussian count is reduced for all reported datasets.

Table 1. Opti3DGS consistently lowers Gaussian count for all reported methods as well as improving the reconstruction quality for some. Note we also report the maximum Gaussian count for methods where it peaks before the end of optimization.

Method	Mip-NeRF360[1]					Tanks & Temples[11]				Deep Blending[7]								
	SSIM ↑	PSNR ↑	LPIPS ↓	(m:s)	#G (10 ⁶) ↓	Peak #G ↓	SSIM ↑	PSNR ↑	LPIPS ↓	(m:s)	#G (10 ⁶) ↓	Peak #G ↓	SSIM ↑	PSNR ↑	LPIPS ↓	(m:s)	#G (10 ⁶) ↓	Peak #G ↓
Compact-3DGS[12]	0.799	27.01	0.242	16:53	1.489	2.605	0.834	23.34	0.199	10:33	0.839	1.472	0.904	29.79	0.254	15:41	1.052	2.300
Compact-3DGS + Ours	0.792	26.96	0.262	13:37	1.048	1.697	0.827	23.26	0.217	08:31	0.601	1.016	0.904	29.81	0.258	13:46	0.831	1.710
Reduced-3DGS[19]	0.810	27.29	0.229	11:55	1.460	-	0.841	23.52	0.186	06:45	0.568	-	0.903	29.63	0.248	11:00	0.925	-
Reduced-3DGS + Ours	0.801	27.14	0.250	09:55	1.061	-	0.834	23.52	0.203	05:38	0.409	-	0.904	29.76	0.251	09:53	0.697	-
Mini-Splatting[4]	0.820	27.25	0.219	11:01	0.496	4.240	0.832	23.22	0.202	07:10	0.203	4.311	0.904	29.88	0.256	10:00	0.352	4.517
Mini-Splatting + Ours	0.821	27.26	0.219	11:21	0.488	4.209	0.834	23.17	0.204	07:13	0.197	4.223	0.908	30.01	0.254	10:07	0.344	4.387
Taming3DGS[15] (budget)	0.793	27.21	0.262	14:36	0.666	-	0.832	23.66	0.213	02:19	0.319	-	0.899	29.75	0.273	02:14	0.294	-
Taming3DGS (budget) + Ours	0.788	27.27	0.274	14:11	0.5735	-	0.834	23.90	0.215	02:17	0.318	-	0.905	30.00	0.269	02:22	0.294	-
Taming3DGS[15] (big)	0.823	27.82	0.207	06:46	3.251	-	0.859	24.14	0.160	05:04	2.290	-	0.909	30.04	0.233	06:15	3.593	-
Taming3DGS (big) + Ours	0.817	27.77	0.223	05:19	2.345	-	0.854	24.22	0.175	03:38	1.333	-	0.911	30.13	0.237	04:57	2.212	-
EAGLES[5]	0.81	27.23	0.24	09:40	1.33	-	0.84	23.27	0.20	06:19	0.65	-	0.91	29.86	0.25	11:22	1.19	-
EAGLES + Ours	0.79	26.90	0.27	13:21	0.90	-	0.83	23.28	0.21	07:00	0.58	-	0.91	29.86	0.25	11:36	0.87	-
3DGS[9]	0.813	27.53	0.221	11:42	3.157	-	0.844	23.69	0.178	07:19	1.825	-	0.900	29.54	0.247	11:34	2.795	-
3DGS + Ours	0.809	27.09	0.237	09:50	1.327	-	0.823	23.15	0.217	05:56	0.658	-	0.902	29.56	0.255	10:26	0.953	-



(a) 3DGS* Error Map [PSNR: 25.20, Gaussians: 6,071,666]



(b) Ours Error Map [PSNR: 25.01, Gaussians: 2,107,227]

Figure 5. Pixel level comparison of error maps against the ground truth image. Our approach maintains similar quantitative scores while using fewer Gaussians and results in a decreased pixel wise error. Note the absence of noise like bright points in our results, due to the removal of tiny redundant Gaussians.

4.2. Efficient use of Gaussian Primitives

For 3DGS [9] our approach reduces the Gaussian primitive count by upto 62% but we also makes more efficient use of any given Gaussian budget, meaning it can derive more quality and a better reconstruction given the same number of Gaussian primitives as shown in Table 1. The ADC in 3DGS generally adds redundant and even wasteful Gaussians in some parts of the scene driving up the compute requirements with no gain in quality [12, 18, 19]. Our method

Table 2. We demonstrate the effectiveness of our image filtering approach compared to EAGLES [6]. We use the default image downsizing based approach with starting resize threshold of 0.3 and duration of 0.7 and apply it to 3DGS [9] to isolate its impact. We report our results from ablation on mean filter with a cosine_restart decay schedule with starting kernel size 15.

Dataset	Method	SSIM ↑	PSNR ↑	LPIPS ↓	#G (10 ⁶) ↓
Mip-NeRF360	EAGLES [5] (resize 0.3)	0.810	27.44	0.232	2.412
Mip-Nekr500	OURS-ablation	0.812	27.45	0.230	2.377
Tanks & Temples	EAGLES [5] (resize 0.3)	0.843	23.59	0.191	1.090
ranks & rempies	OURS-ablation	0.844	23.65	0.188	1.359
Deep Blending	EAGLES [5] (resize 0.3)	0.904	29.55	0.247	2.325
Беер Біенанід	OURS-ablation	0.905	29.64	0.245	2.298

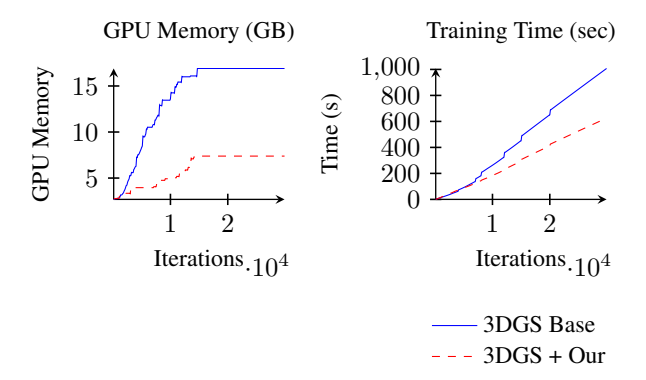


Figure 6. We reduce the GPU memory required during optimization due to a reduced Gaussian primitive load, which also reduces the total optimization time. These results are for 3DGS[9] across the bicycle scenes and are representive of all scenes tested.

reduces the wasteful and redundant use of Gaussians as well and drives the quality higher as shown by the lack of bright noise pattern seen in Figure 5.

4.3. Ablations

Modulation Schedule: We experiment with various frequency modulation schedules in Figure 8a. The results indicate that the step schedule function works better than linear, exponential, or cosine variants across all scenes in the

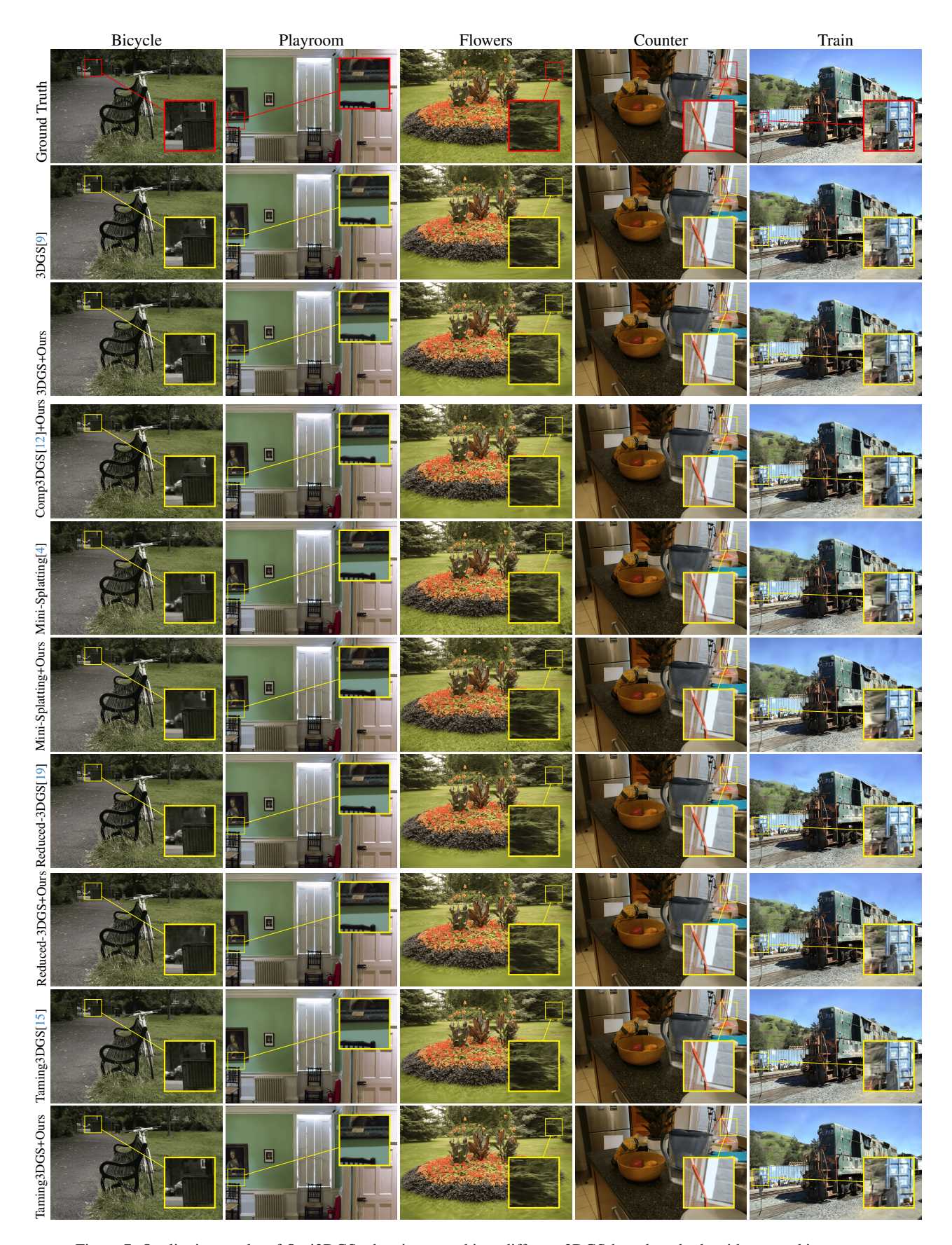


Figure 7. Qualitative results of Opti3DGS when integrated into different 3DGS-based methods with zoomed in cut-outs.

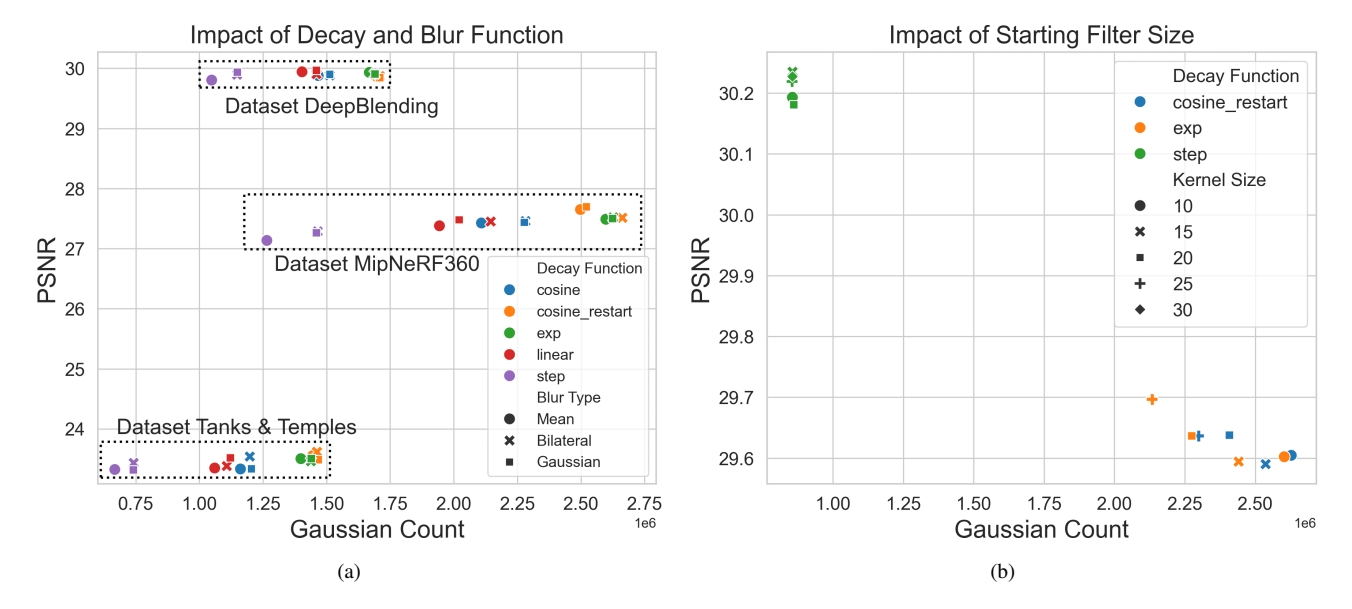


Figure 8. Ablation Experiments: (a) shows the impact of using different decay rate functions to control the size of the kernel used for image filtering. Combining step decay function with the mean filter performs best and is adopted across all our experiments. Note each point is the average score for that respective dataset. (b) shows the impact of using different initial kernel sizes with the mean filter. Larger starting kernel size reduces the Gaussian count but the quality plateaus.

datasets by a significant margin.

Blur Filter: We also test various types of image filtering algorithms including Gaussian, bilinear and mean filtering to determine the best approach. The results, shown in Figure 8a, indicate that the mean filter performs well on most type of scenes. Surprisingly Gaussian and bilateral filtering perform poorly as they gives more weight to the pixel at the center of the kernel or to edge information in the images. **Kernel Size**: Holding the step function constant and using a mean filter, we perform experiments to evaluate the impact of the image filtering intensity on the final reconstruction quality. Results, shown in Figure 8b, indicate that starting from a larger filter improves performance but the trend peaks quickly. We adopt the step decay function with an initial kernel size of 15 in all our experiments for the first 12_000 iterations.

5. Conclusions

Summary: We have presented Opti3DGS, a simple yet highly effective framework that minimizes the number of Gaussian primitives in 3DGS-based pipelines. We demonstrated an average reduction of 62% in Gaussian count, a 40% reduction in the training GPU memory requirements and a 20% reduction in optimization time without sacrificing the visual quality compared to 3DGS [9]. We have conducted an extensive quantitative and qualitative evaluation that has shown Opti3DGS can be seamlessly integrated into a wide range of current 3DGS-based approaches resulting in a positive impact on primitive count in all cases. The

contribution of Opti3DGS enables 3DGS-based pipelines and scene reconstructions to be more usable on a range of consumer-grade devices due to reduced primitives and therefore storage, transmission and utilization requirements making the technology more widely accessible.

Limitations: Currently Opti3DGS is agnostic to the image content and applies filtering on the entire training set uniformly, but it fails to take into account structural boundaries and large constant object which could be better represented by singular Gaussians with the right pixel level emphasis. A content-aware extension will be considered in the future. Future Work will focus on using edge and depth aware image filtering operations and investigating the impact of using projected Gaussian centroid density in the image space to selectively guide attention to areas with lower visual variation which remain poorly densified by the ADC. We will also explore the extension of Opti3DGS to dynamic scenes exploiting the level-of-detail representation.

References

- Jonathan T. Barron, Ben Mildenhall, Dor Verbin, Pratul P. Srinivasan, and Peter Hedman. Mip-nerf 360: Unbounded anti-aliased neural radiance fields. CVPR, 2022. 5, 6
- [2] Chenxi Lola Deng and Enzo Tartaglione. Compressing explicit voxel grid representations: fast nerfs become also small. In *Proceedings of the IEEE/CVF Winter Conference on Applications of Computer Vision*, pages 1236–1245, 2023. 1
- [3] Zhiwen Fan, Kevin Wang, Kairun Wen, Zehao Zhu, Dejia Xu, and Zhangyang Wang. Lightgaussian: Unbounded 3d gaussian compression with 15x reduction and 200+ fps. arXiv preprint arXiv:2311.17245, 2023. 2
- [4] Guangchi Fang and Bing Wang. Mini-splatting: Representing scenes with a constrained number of gaussians. *arXiv* preprint arXiv:2403.14166, 2024. 1, 2, 5, 6, 7
- [5] Sharath Girish, Kamal Gupta, and Abhinav Shrivastava. Eagles: Efficient accelerated 3d gaussians with lightweight encodings. arXiv preprint arXiv:2312.04564, 2023. 1, 2, 5, 6
- [6] Sharath Girish, Kamal Gupta, and Abhinav Shrivastava. Eagles: Efficient accelerated 3d gaussians with lightweight encodings. In *European Conference on Computer Vision*, pages 54–71. Springer, 2024. 6
- [7] Peter Hedman, Pratul P. Srinivasan, Ben Mildenhall, Jonathan T. Barron, and Paul Debevec. Baking neural radiance fields for real-time view synthesis, 2021. 5, 6
- [8] Tao Hu, Shu Liu, Yilun Chen, Tiancheng Shen, and Jiaya Jia. Efficientnerf efficient neural radiance fields. In Proceedings of the IEEE/CVF Conference on Computer Vision and Pattern Recognition, pages 12902–12911, 2022. 1
- [9] Bernhard Kerbl, Georgios Kopanas, Thomas Leimkühler, and George Drettakis. 3d gaussian splatting for real-time radiance field rendering. ACM Transactions on Graphics, 42 (4):1–14, 2023. 1, 2, 3, 5, 6, 7, 8
- [10] Sieun Kim, Kyungjin Lee, and Youngki Lee. Color-cued efficient densification method for 3d gaussian splatting. In Proceedings of the IEEE/CVF Conference on Computer Vision and Pattern Recognition, pages 775–783, 2024. 2
- [11] Arno Knapitsch, Jaesik Park, Qian-Yi Zhou, and Vladlen Koltun. Tanks and temples: Benchmarking large-scale scene reconstruction. ACM Transactions on Graphics, 36(4), 2017.
 5, 6
- [12] Joo Chan Lee, Daniel Rho, Xiangyu Sun, Jong Hwan Ko, and Eunbyung Park. Compact 3d gaussian representation for radiance field. *arXiv preprint arXiv:2311.13681*, 2023. 1, 2, 5, 6, 7
- [13] Ruilong Li, Hang Gao, Matthew Tancik, and Angjoo Kanazawa. Nerfacc: Efficient sampling accelerates nerfs. In *Proceedings of the IEEE/CVF International Conference on Computer Vision*, pages 18537–18546, 2023. 1
- [14] Xiangrui Liu, Xinju Wu, Pingping Zhang, Shiqi Wang, Zhu Li, and Sam Kwong. Compgs: Efficient 3d scene representation via compressed gaussian splatting. arXiv preprint arXiv:2404.09458, 2024.
- [15] Saswat Subhajyoti Mallick, Rahul Goel, Bernhard Kerbl, Markus Steinberger, Francisco Vicente Carrasco, and Fer-

- nando De La Torre. Taming 3dgs: High-quality radiance fields with limited resources. In *SIGGRAPH Asia 2024 Conference Papers*, pages 1–11, 2024. 1, 2, 6, 7
- [16] Ben Mildenhall, Pratul P Srinivasan, Matthew Tancik, Jonathan T Barron, Ravi Ramamoorthi, and Ren Ng. Nerf: Representing scenes as neural radiance fields for view synthesis. *Communications of the ACM*, 65(1):99–106, 2021.
- [17] KL Navaneet, Kossar Pourahmadi Meibodi, Soroush Abbasi Koohpayegani, and Hamed Pirsiavash. Compact3d: Compressing gaussian splat radiance field models with vector quantization. arXiv preprint arXiv:2311.18159, 2023. 2
- [18] Simon Niedermayr, Josef Stumpfegger, and Rüdiger Westermann. Compressed 3d gaussian splatting for accelerated novel view synthesis. *arXiv preprint arXiv:2401.02436*, 2023. 2, 6
- [19] Panagiotis Papantonakis, Georgios Kopanas, Bernhard Kerbl, Alexandre Lanvin, and George Drettakis. Reducing the memory footprint of 3d gaussian splatting. *Proceedings of the ACM on Computer Graphics and Interactive Techniques*, 7(1):1–17, 2024. 1, 2, 6, 7
- [20] Henan Wang, Hanxin Zhu, Tianyu He, Runsen Feng, Jiajun Deng, Jiang Bian, and Zhibo Chen. End-to-end ratedistortion optimized 3d gaussian representation. arXiv preprint arXiv:2406.01597, 2024. 2
- [21] Jiahui Zhang, Fangneng Zhan, Muyu Xu, Shijian Lu, and Eric Xing. Fregs: 3d gaussian splatting with progressive frequency regularization. *arXiv preprint arXiv:2403.06908*, 2024. 3
- [22] Hexu Zhao, Haoyang Weng, Daohan Lu, Ang Li, Jinyang Li, Aurojit Panda, and Saining Xie. On scaling up 3d gaussian splatting training. arXiv preprint arXiv:2406.18533, 2024.